Journal of Electronic Materials, Vol. 21, No. 6, 1992

Characterization of Eutectic Sn-Bi Solder Joints

Z. MEI and J. W. MORRIS, Jr.

Center for Advanced Materials, Lawrence Berkeley Laboratory and Department of Materials Science and Mineral Engineering, University of California, Berkeley, CA 94720

This report presents experimental results on 58Bi-42Sn solder joints, optical and SEM microstructures of their matrix and of their interface with copper, solidification behavior studied by differential scanning calorimetry, wettability to copper, creep, and low cycle fatigue. These results are discussed in comparison with 60Sn-40Pb solder, and with three low temperature solders, 52In-48Sn, 43Sn-43Pb-14Bi, and 40In-40Sn-20Pb. The 58Bi-42Sn solder paste with RMA flux wets Cu matrix with a wetting angle of 35° and had a 15° C undercooling during solidification. The constitutive equation of the steady state shear strain rate, and the Coffin-Manson relation constants for the low cycle shear fatigue life at 65° C have been determined. The test results show that this solder has the best creep resistance but the poorest fatigue strength compared with the other four solders.

Key words: Low temperature solders, bismuth-tin solder

I. INTRODUCTION

The eutectic 58Bi-42Sn alloy is a possible solder for use in low temperature soldering. Low temperature soldering refers to the soldering at temperatures between 170–200° C,[1-4] as compared to the usual soldering temperatures around 250° C with eutectic or near-eutectic Sn-Pb solders of the melting points around 183° C. Low temperature soldering is necessary when electronic devices to be soldered are prone to thermal damage. It can also reduce the risk of thermal shock induced by the thermal expansion mismatch among different materials in an electronic package. Step soldering is another application for low temperature solders and is commonly used when soldering a device requires more than one step; the solder used for subsequent step should have a lower melting point than that used for the previous step.

Low temperature solders are usually cadmium-, indium- or bismuth-containing alloys that have melting points ranging between 45° C–170° C.[5-7] The toxicity of Cd-containing solders makes them unsuitable for industrial use. The feasibility for lower temperature soldering of both In- and Bi-containing solders has been tested, but In-containing solders are relatively more expensive.

Despite their increased applications in the electronic packaging industry, the mechanical properties of low temperature solders have not been well studied. Solder joints made of four different alloys (in weight percent) 58Bi-42Sn (eutectic), 52In-48Sn (eutectic), 43Sn-43Pb-14Bi, and 40In-40Sn-20Pb, have been characterized in this laboratory. The results of creep tests of the last three solders listed above were reported previously.[8] This article presents the results on 58Bi-42Sn solder joints, the optical microstructure of the matrix and of the interface with copper, solidification behavior studied by differential scanning calorimetry (*DSC*), wettability to copper, creep, and low cycle fatigue. These results are discussed in comparison with near-eutectic 60Sn-40Pb solder and with the other three low temperature solders.

The 58Bi-42Sn alloy melts at 139° C.[9] This alloy has been known and used for a long time as a casting and pattern alloy, distinguished by its excellent mobility in the molten state, and especially a zero shrinkage upon solidification. Other physical and mechanical properties of this alloy published in the literature[4,7,10,11] are listed in Table I. The alloy has a stronger shear strength and longer joint life than the eutectic Sn-Pb solder at temperatures between 20°–70° C.[4] Fatigue life study by Wild[12] showed that the eutectic Bi-Sn alloy was less fatigue resistant than the eutectic Sn-Pb solder. The wettability of this alloy on a Cu matrix was comparable with that of the eutectic Sn-Pb solder when a newly developed flux was used.[3]

II. EXPERIMENTAL PROCEDURES AND RESULTS

The chemical composition of the 58Bi-42Sn alloy used in this study is listed as 58.0 wt.% Bi, 42.0 wt.% Sn, with impurities of 15 ppm Ag, 20 ppm In, <2 ppm Cd, <2 ppm Ni, 10 ppm Cu, 75 ppm Sb, 5 ppm Fe, 2 ppm Tl, and 500 ppm Pb. The alloy was provided by Indium Corp. of America in the form of solder paste which is a blend of 88 wt.% metallic powder sized between 44 to 74 μm (mesh −200/+325) and 12 wt.% mildly activated rosin flux (type RMA).

DSC Tests

Differential scanning calorimetry (*DSC*) was used to characterize temperatures and the kinetics for melting and solidification of solder paste. In a *DSC*, two sample holders, one with a drop of solder paste and one without, are heated up and cooled down. The difference in the absorbed heat between two holders is recorded as function of temperature. When

(Received November 22, 1991; revised February 27, 1992)

0361-5235/1992/1401-599$5.00©92 TMS

Table I. Some Physical and Mechanical Properties of Eutectic Sn-Bi Alloy

Melting Point (°C)	Density (kg/m^3)	Vlmn Change Liquid to Solid	Specific Heat (cal/g/°C)	Thermal Expansion (mm/mm/°C)
138 Ref. 9	8700 Ref. 10	+0.77% Ref. 10	0.045 Ref. 10	0.000015 Ref. 10

Surface Tension (dyne/cm)	Hardness (HB)	Shear Strength (N/mm^2)	Shear Strength (N/mm^2)
391 Ref. 11	22 Ref. 11	50 (at 20° C) Ref. 7	19.5 (100° C) Ref. 7

the difference is positive, the solder paste is undergoing an endothermic reaction, and vice versa. The heating and cooling rates of the *DSC* were set to be 40° C/min which are close to the heating rate of the furnace that was used to make solder joints for creep and fatigue tests. A solder paste sample was heated from low to high temperatures until it melted and then cooled to low temperature through solidification; the heating and cooling cycle was repeated three times.

Figure 1(a) plots the *DSC* result of a 58Bi-42Sn solder paste sample. The curves of the second and third heating-cooling cycles are very close, but they are different from that of the first cycle. This is due to the presence of the flux in solder paste during the first heating-cooling process. There is only one peak during heating and one dip during cooling in Fig. 1(a), indicating melting and solidification processes. The Sn-Bi phase diagram[9] indicates that the eutectic 58Bi-42Sn alloy melts and solidifies at a single temperature, 139° C; the *DSC* curve of 58Bi-42Sn alloy shows that the alloy started to melt at about 140° C and finished at about 160° C. The alloy did not begin to solidify until being cooled below 123° C. Figures 1(b–e) include *DSC* curves for eutectic Sn-Pb and Sn-In, and non-eutectic 40In-40Sn-20Pb and 43Sn-43Pb-14Bi solder pastes. It is noticed that the undercoolings (defined here as the difference between the melting start temperature and solidification start temperature) for the three eutectic alloys are about 10 to 20° C, while those for the two non-eutectic alloys are nearly zero.

Wettability Tests

Wetting balance is the most advanced technique nowadays for wettability testing. Because only a limited amount of solder paste was available to us, this technique was not used. Instead, a simple test method was adopted in this study to determine the wetting angle, α, by measuring the height, h, and the diameter, L, of a solder joint cap, as explained in Appendix I. The wettability tests proceeded as follows: etching a copper plate by dipping it into Johnsons Stainless Steel Flux (which consisted of a dilute solution of zinc chloride and hydrochloric acid); cleaning the Cu plate with alcohol; delivering solder paste from a syringe onto the copper plate; reflowing the paste on the copper plate in a furnace at 20° C above the liquidus temperature of the tested paste for three minutes; measuring the height and diameter of the solidified solder drop. The other four alloys as well as the eutectic Sn-Bi were tested, at least eight times for each solder.

The values of the wetting angle and its standard deviation for the five alloys are listed as: 58Bi-42Sn, 35.42° ± 1.95°; 43Sn-43Pb-14Bi, 15.93° ± 1.72°; 40In-40Sn-20Pb, 27.58° ± 3.04°; 52In-48Sn, 28.13° ± 1.72°, and 63Sn-37Pb, 24.67° ± 2.03°. Since the resulting wetting angles are all <90°, all solder pastes are wettable with copper. Among the five solders, the eutectic Sn-Bi was the worst, when the same flux (RMA) was used. It is interesting to observe that 58Bi-42Sn solder beads after solidification have "shiny" looks, the surface of the solder beads are very smooth and light-reflective. This phenomenon is probably related with the oxide-free melting behavior mentioned in Ref. 4.

Optical Microstructure

Solder joints made by reflowing solder paste (as described later in the Creep Tests section) were cut using an ISOMET diamond blade saw to expose the solder joint cross section. Specimens were then cold-mounted, ground, mechanically polished with light pressure, and then observed under an optical microscope.

Pictures in Fig. 2 show the lamellar structures of this alloy. The two pictures show the same area of a joint, however, the top picture was taken when the joint was as-polished, while the bottom one was taken after the joint had been etched with a solution of 93% methanol, 5% HNO_3, and 2% HCl. Because it attacks Sn-rich phase only, the etchant reversed the contrast of the two pictures. Therefore, the darkly and lightly colored areas in the bottom picture are the Sn-rich and Bi-rich phase regions, respectively; and vice versa in the top picture. It is noticed that at the top left or bottom right corners in the pictures, there are some small and round dots; they are probably the Bi-precipitate particles in the Sn-rich phase. The phase diagram of this alloy indicates that the solubility of Bi in Sn reduces sharply from 21 wt.% at the melting point (139° C) to about 4 wt.% at 20° C.

The lamellar structure of the eutectic Bi-Sn is similar to that of the eutectic Sn-Pb with some differences. The volume ratio of the Pb-rich phase to Sn-rich phase in the eutectic 37Pb-63Sn is about

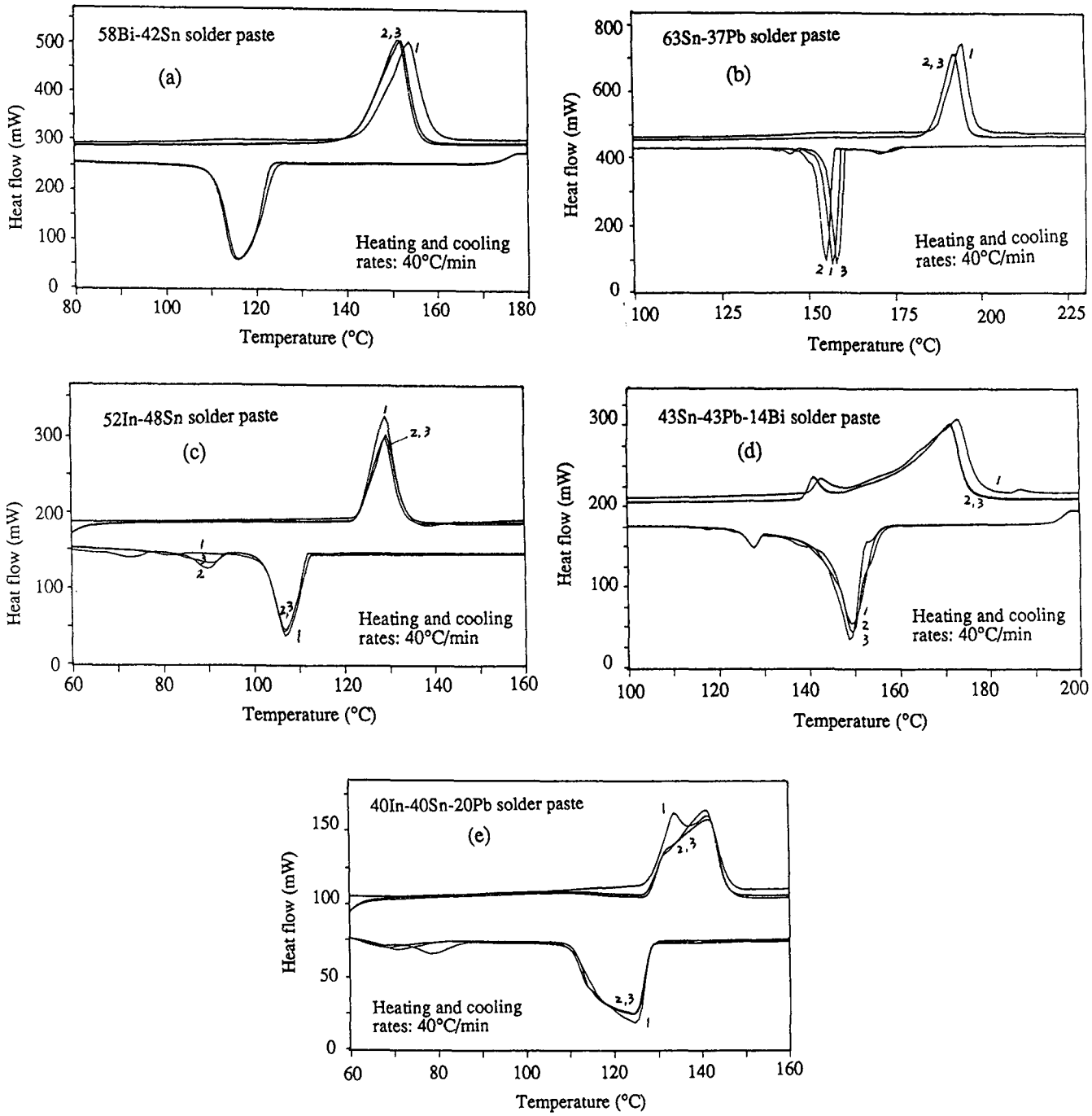

Fig. 1 — Differential Scanning Calorimeter results (three runs indicated as 1, 2, and 3) of five solder pastes: three eutectic, (a) 58Bi-42Sn (b) 63Sn-37Pb and (c) 52In-48Sn; and two non-eutectic, (d) 43Sn-43Pb-14Bi and (e) 40In-40Sn-20Pb.

27:73; while the volume ratio of the Sn-rich phase to the Bi-rich phase in the eutectic 42Sn-58Bi is about 49:51. In an optical picture of the eutectic Sn-Pb, the Pb-rich phase is seen to reside in a matrix of the Sn-rich phase; while in a picture of the eutectic Bi-Sn, the Bi- and Sn-rich phases are more mutually related. Colony boundaries are more difficult to recognize in the eutectic Bi-Sn solder. Sometimes, η-phase (Cu_6Sn_5) can be found in a eutectic Sn-Pb solder joint with Cu matrix, but η-phase was never seen in the eutectic Sn-Bi solder joints with Cu matrix that were observed in this study.

SEM Microstructure

The scanning electron microscope is used to characterize solder joint microstructure because of its higher magnification power and chemical analysis capability. The picture of Fig. 3(a) is a secondary electron image, showing an interfacial area between 58Bi-42Sn solder (on the right side) and copper (on the left side). The pictures on Fig. 3(b)–(d) are the elemental x-ray maps for Bi, Sn and Cu, respectively, taken on the same area of Fig. 3(a). Comparing these pictures leads to the following observations.

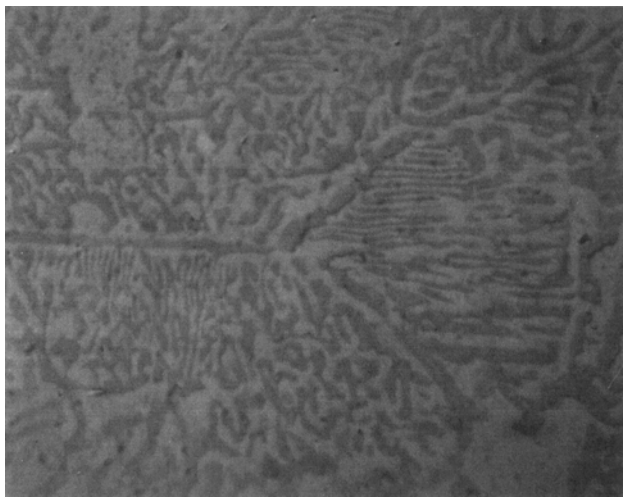

Fig. 2 — Optical micrographs of a 58Bi-42Sn solder joint, (a) as-polished, and (b) etched with a solution of (2% HCl, 5% HNO_3, 93% methanol). Notice the reversed contrasts between the two graphs, indicating that the etching solution attacks only the Sn-rich phase not the Bi-rich phase.

(1) The Sn- and Bi-maps are complementary. Inside the Sn-rich phase small precipitate particles are visible in the secondary electron image, while the Bi-rich phase areas are very clean.

(2) At the interface between Cu and the solder, the Cu-map has a tooth-match with the Sn-map but not with Bi-map. This indicates that the intermetallic layer formed between Cu and the solder is a product of Cu with Sn but not Cu with Bi. The Cu-Bi binary phase diagram[9] shows that there is no intermetallic phase between Bi and Cu, and Cu and Bi are essentially mutually insoluble under 270° C. Only a metastable compound, Cu_5Bi_2, has been previously reported.[13] On the other hand, Sn and Cu may form Cu_3Sn and Cu_6Sn_5 intermetallics.[9] It is impossible, however, to tell from Fig. 3(a–d) whether there is one or two phases in the interfacial layer.

(3) Cu atoms can be found a few microns deep from the interface into the solder, as seen from the Cu map. Cu atoms dissolve into the solder matrix when the solder is molten, or diffuse into it after solidification. It has been reported that Cu atom can diffuse at low temperatures through pure Sn very rapidly due to its interstitial diffusion mechanisms.[14–16] The interstitial diffusion usually has a smaller activation energy than the substitutional diffusion, and is probably responsible for the fast diffusion of Cu inside the Bi-Sn solder.

Creep Tests

A detailed description on specimen preparation and the creep test facility has been provided elsewhere.[17,18] The geometry and size of the double-shear specimens are shown schematically in Fig. 4(a). Solder joints are sandwiched between three plates of printed circuit board made of epoxy fiber glass coated with a patterned pure copper film. Solder joints were formed by reflowing solder paste in a furnace at 120° C for 5 min, 170° C for 3 min, following by air-cool.

Figure 5 shows a typical creep test curve of a 58Bi-42Sn solder joint specimen; it has three stages: primary, steady state, and tertiary. This is different from the creep curves of the eutectic In-Sn or 40In-40Sn-20Pb solders which exhibit no primary creep.[8]

The steady state strain rate, $d\gamma/dt$, depends on the applied stress τ, and temperature T (in Kelvin scale) according to Power Law[19]

$$\frac{d\gamma}{dt} = A\tau^n \exp\left(-\frac{\Delta H}{RT}\right), \qquad (1)$$

where ΔH is the activation energy, R is the gas constant, and A is a pre-exponential factor depending on microstructure. In order to evaluate the parameters in Equation (1), the steady state strain rates were determined at the three temperatures 20, 65 and 90° C. At each temperature, the steady state strain rates at more than five different stress levels were measured and ranged between 10^{-7} (1/sec) to 10^{-3} (1/sec). Figure 6 plots the steady state strain rates versus the applied shear stresses at the three temperatures on a log-log scale. The slope of the linear curve fitting through the data points of one temperature gives an evaluation of the stress exponents n, in Eq. (1).

The value of the stress exponent is an indication of the creep deformation mechanisms.[20] For most metals, the stress exponents are between 4 to 7 when they creep through dislocation climb; or are close to 2 when they creep by grain boundary sliding which is the mechanism for superplasticity. It is seen from the curves in Fig. 6 that the stress exponents of 58Bi-42Sn at 20°, 65°, and 90° C are between 4.1 and 4.6. The eutectic In-Sn and 40In-40Sn-20Pb solders, on the other hand, exhibit stress exponent values between 2 and 3.[8]

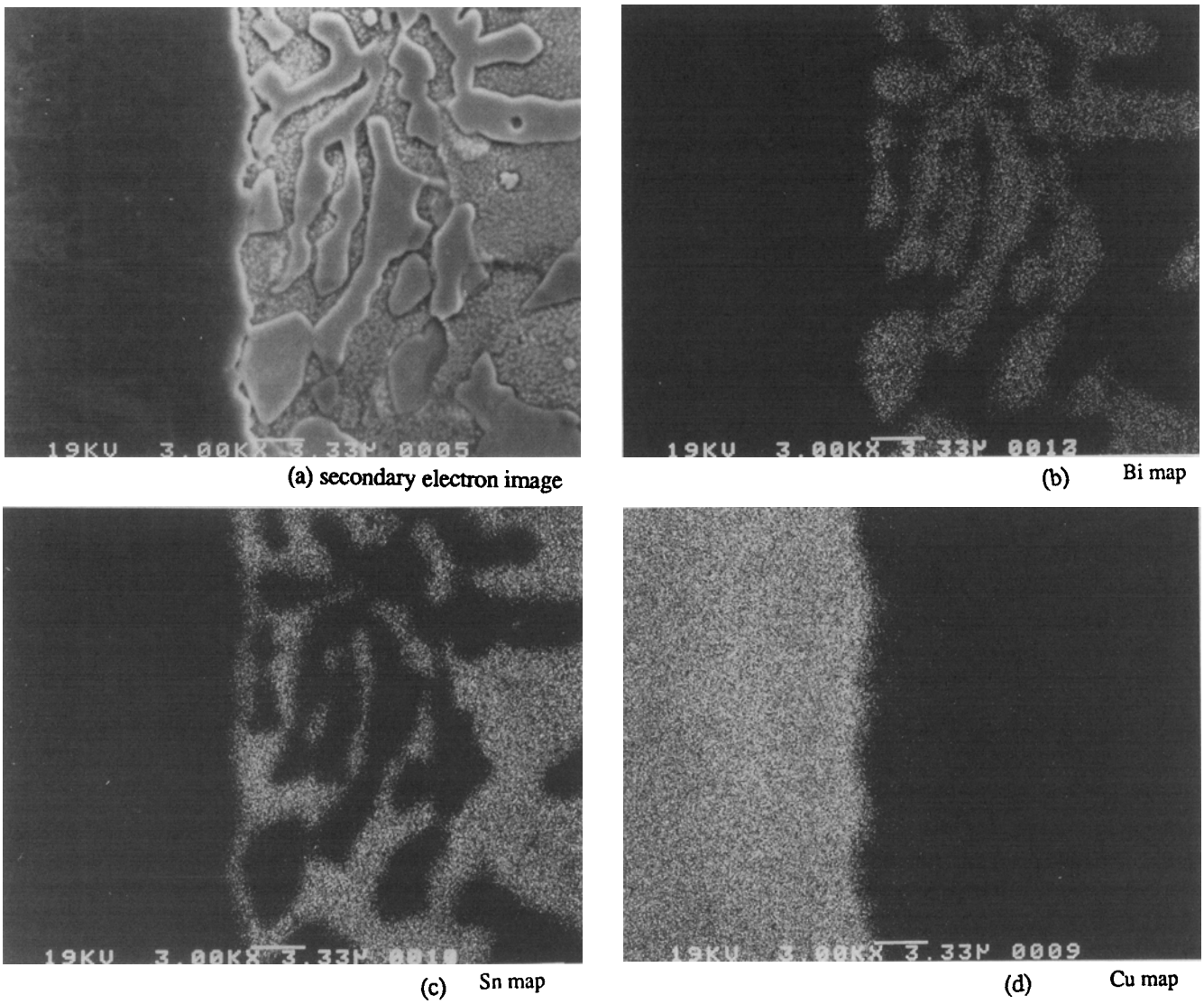

Fig. 3 — (a) Secondary electron image of a 58Bi-42Sn solder joint and its x-ray elementary maps of (b) Sn (c) Bi and (d) Cu.

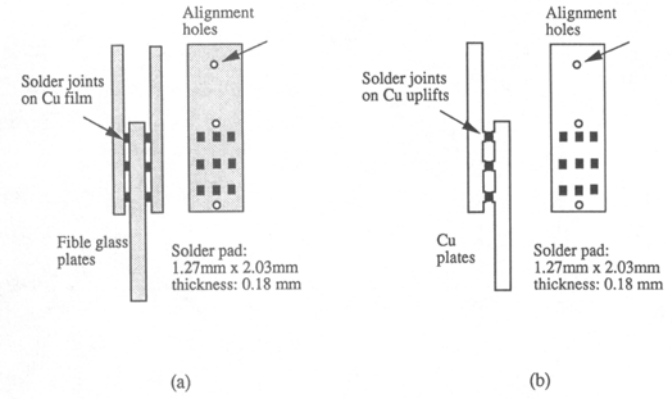

Fig. 4 — (a) double-shear and (b) single-shear specimens for creep and fatigue tests of solder joints, respectively.

The activation energy as well as the other parameters in Eq. (1) for the eutectic Sn-Bi solder were estimated by the least-square curve fitting of the strain rates vs shear stress data at all three temperatures. The values of the thus determined parameters are,

$$\frac{d\gamma}{dt}(1/\text{sec}) = 5.5403 \times 10^{-7}\,\tau^{4.0514} \exp\left(-\frac{16.852)}{RT}\right) \qquad (2)$$

where τ and ΔH have the units of psi and Kcal/mole, respectively. The quality of the curve-fitted can be seen in Fig. 7 where the normalized steady state strain rates, $d\gamma/dt \exp(\Delta H/RT)$, versus applied shear stresses are plotted for the data at the three different temperatures. If the curve-fitted activation energy and other parameters are correct, the normal-

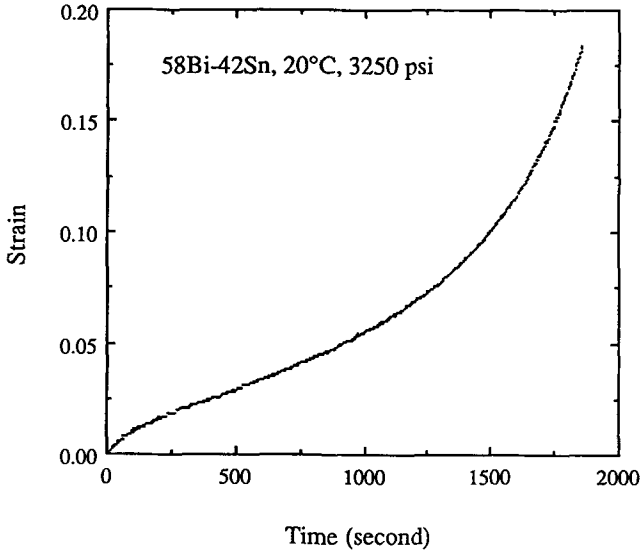

Fig. 5 — A typical curve of creep tests of 58Bi-42Sn solder joints.

ized strain rates versus applied stress curves at 20°, 65°, and 90° C should be co-linear, and the linear line should be closely represented by Eq. 2.

Figure 8 compares the data of steady state shear strain rates vs shear stresses at 65° C of the eutectic Bi-Sn solder with the other three low temperature solders and the 60Sn-40Pb solder. It is seen that the eutectic 58Bi-42Sn is the strongest among the five solders. The strain rates under the same stress vary more than three orders of magnitude between the softest eutectic In-Sn and the hardest eutectic Bi-Sn. Ductility of the eutectic Sn-Bi solder joints, however, was only about 20–25% in contrast with more than 60% for the 43Sn-43Pb-14Bi solder, more than 100% for the eutectic 52In-48Sn solder, and more than 150% for 40In-40Sn-20Pb solder.[8]

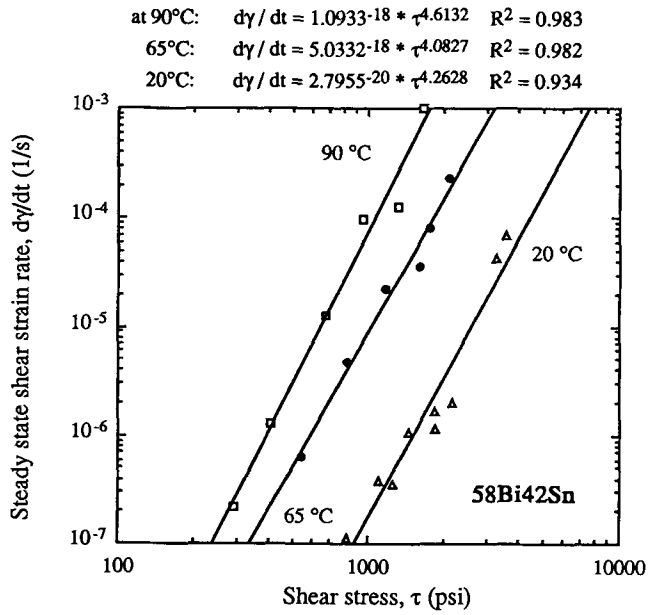

Fig. 6 — Creep test results of steady state strain rate vs shear stress for 58Bi-42Sn solder joints tested at 20, 65 and 90° C.

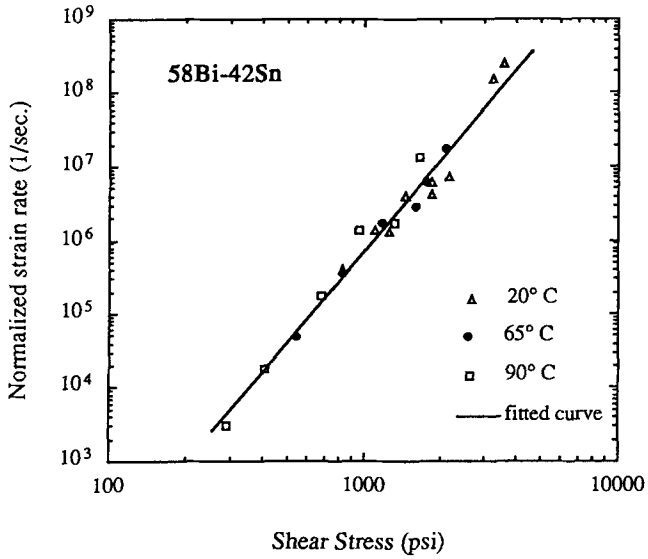

Fig. 7 — Plots of the normalized shear strain rate ($d\gamma/dt \exp(\Delta H/RT)$) vs shear stress determined for 58Bi-42sn solder joints tested at 20, 65 and 90° C. The fitted curve is expressed as Eq. (2) in the text.

Low Cycle Fatigue Tests

The geometry and size of the single-shear specimens shown schematically in Fig. 4(b) are used for shear fatigue tests. Specimens for fatigue tests were made in a method similar to that for creep test specimens with some modifications. The detailed information has been provided elsewhere.[21,22] In fatigue tests, solder joint specimens were strained back and forth cyclically at constant strain amplitude and constant temperature. The load amplitude (maximum load-minimum load) of each cycle was recorded as a function of the cycle number. The fatigue life is defined as the cycle after which the load amplitude drops to 50% that of the initial cycle, as

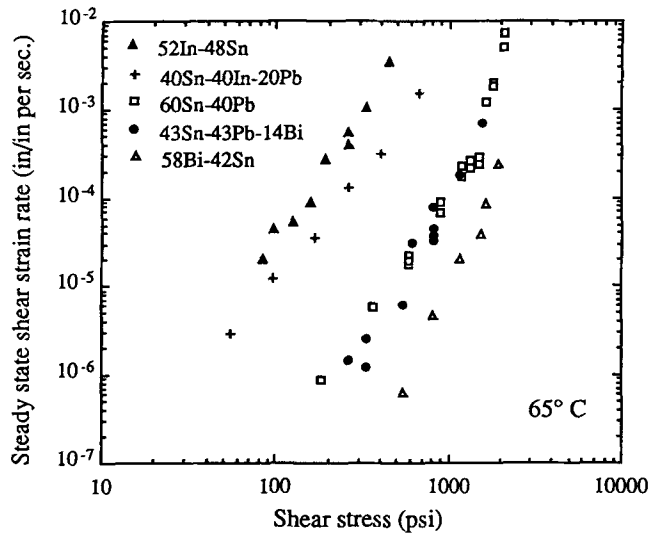

Fig. 8 — Comparison of creep test results at 65° C of five solder alloys. Data for the 52In-48Sn, 40Sn-40In-20Pb and 43Sn-43Pb-14Bi are from Ref. [8], data for the quenched 60Sn-40Pb are from Ref. [18].

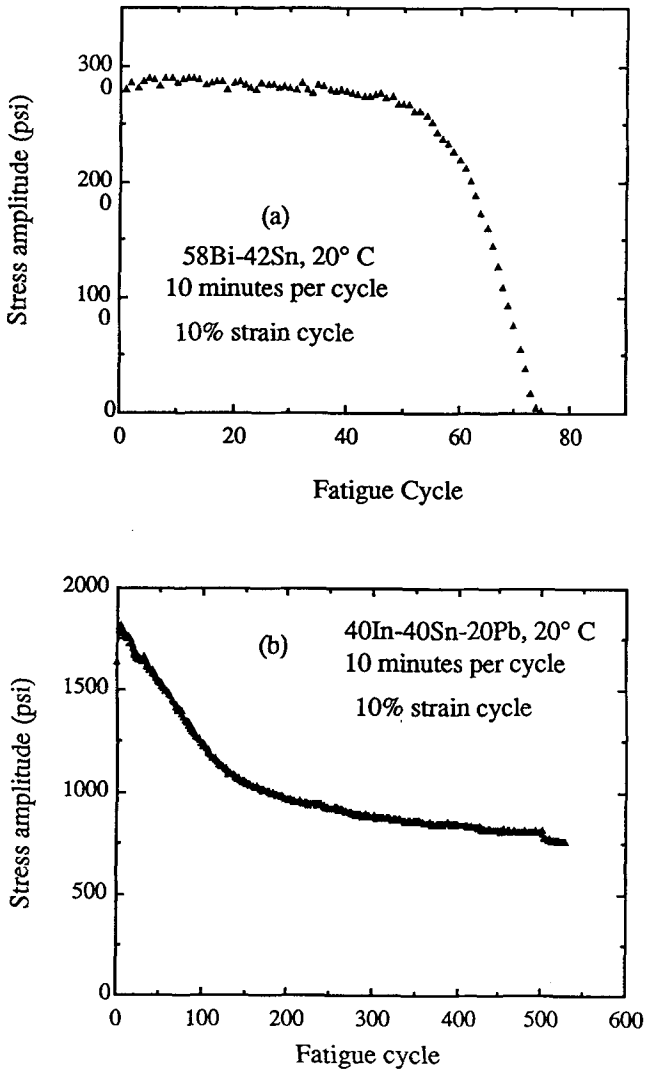

Fig. 9 — Stress amplitudes (= maximum stress − minimum stress in a loading cycle) versus loading cycles recorded in the strain-controlled (10% strain for every cycle) fatigue tests of (a) 58Bi-42Sn and (b) 40In-40Sn-20Pb solder joints, showing different curve shapes for the two solders.

suggested by Solomon.[23] The frequency of the tests are slow, roughly 10 min per cycle, with the strain rate on the order of 10^{-4} 1/sec. A saw-tooth strain versus time profile is used. The shear strain is defined as the displacement/solder joint thickness. The total strain amplitude during a fatigue cycle, $\Delta\gamma$, is defined as the amount of strain between the minimum load and maximum load.

Figure 9(a) shows a typical fatigue test result for 58Bi-42Sn solder joints. It is seen that the load amplitude stayed relatively constant during initial loading cycles, then decreased to zero with an accelerated speed. This appeared to be a result of crack initiation and then propagation. The In-containing solders (52In-48Sn and 40In-40Sn-20Pb), on the other hand, demonstrate an opposite appearance of load amplitude versus cycle plot as shown in Fig. 9(b); the load amplitude decreased quickly at the beginning cycles, and gradually slowed afterwards.

Low cycle fatigue life (N_f) versus applied plastic

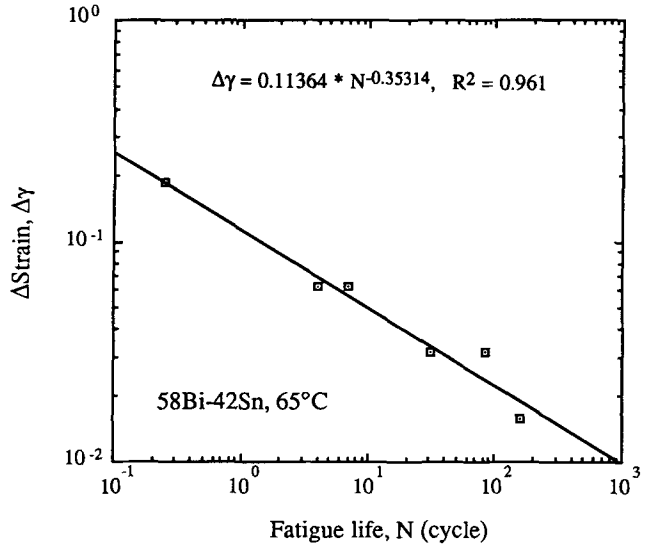

Fig. 10 — Fatigue lives, N (defined as the number of cycles after which the stress amplitude drops to 50% of that at the initial cycle), vs strain amplitudes of strain-controlled fatigue tests of 58Bi-42Sn solder joints at 65° C.

strain ($\Delta\gamma_p$) data are usually described by the Coffin-Manson law[24,25]

$$(N_f)^{\alpha}\Delta\gamma_p = \theta \qquad (3)$$

where θ is a constant related with the ductility, the exponent α is also a constant typically found to be close to 0.5. In this study, however, fatigue tests were controlled by the total strain instead of plastic strain. Therefore fatigue lives N_f as function of the total strain $\Delta\gamma$ were determined at 65° C and shown in Fig. 10. The α and θ constants are evaluated to be equal to 0.35 and 0.114, respectively. The value of α is less than 0.5, but similar values (0.37 for example) were reported elsewhere for 60Sn-40Pb solder.[26]

Figure 11 compares fatigue lives at 20° C for $\Delta\gamma$ = 10% of five solders. The 58Bi-42Sn solder is better than only the 52In48Sn solder and not comparable with the other three solders.

DISCUSSION

This study describes some properties of the eutectic Bi-Sn alloy, one of low temperature solders, in its joint form, and compares this alloy with the other three low temperature solder alloys and with 60Sn-40Pb solder that is not a low temperature solder but extensively used in the electronic packaging industry. The Bi-Sn solder is distinct from the other solders in its high strength (shown by its slow creep strain rate) but poor ductility and fatigue resistance (shown by the isothermal strain-controlled fatigue tests). A recently raised concern in the electronic packaging industry is the thermal fatigue that occurs when materials connected by solder joints have different thermal expansion coefficients. From this point of view, the eutectic Bi-Sn is not recom-

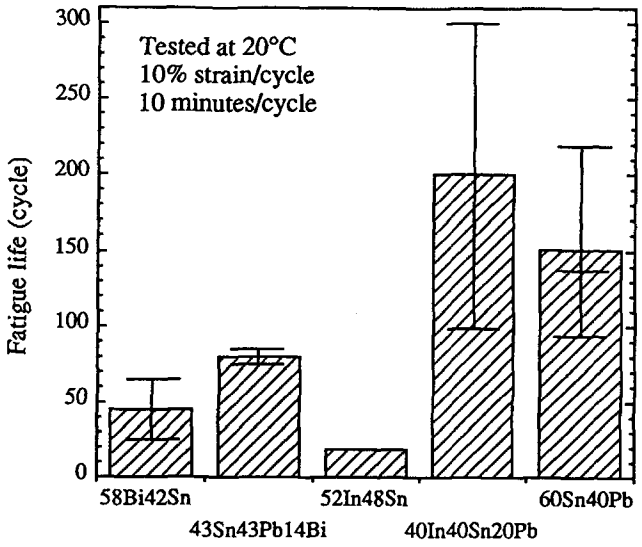

Fig. 11 — Comparison of average fatigue lives (indicated by the heights of shaded columns) of five solders. The bars on the columns indicate fatigue lives of individual tests.

mended as a good low temperature solder in comparison with the other low temperature solders, for example 40In-40Sn-20Pb and 43Sn-43Pb-14Bi as shown in Fig. 11.

The strong and brittle features of the Bi-Sn solder are related with its as-solidified lamellar microstructure. The deformation of an alloy at high homologous temperatures (T/melting T) can be accomplished by either dislocation movements (glide and climb) or grain and interface boundary movement (rotation and slide). In a as-solidified eutectic Bi-Sn solder joint, the Sn-rich and Bi-rich phases are weaved into mutually tangled lamellar arrangements which make the dislocation passage from one phase to another difficult. The relative movement at the interphase boundaries is also difficult because the affinity between the certain crystallographic planes of the Sn-rich phase and Bi-rich phase that developed during side-by-side eutectic growth in solidification. However, if its lamellar strucuture is replaced with an equiaxed grain structure by cold-work and recrystallization, this alloy can be very soft and ductile. In fact, the 58Bi-42Sn alloy is one of the earliest discovered superplastic alloys, along with eutectic Sn-Pb alloy,[27] after the alloy was extruded.

It was found in *DSC* tests that during solidification three eutectic solder alloys have 10–20° C undercooling while two non-eutecitic alloys have almost zero undercooling. The reason is not known. The undercooling is usually required by the nucleation energy for the new solid phase forming inside the liquid solders, it is not known why the eutectic phases have higher nucleation energies than the non-eutectic phases.

SUMMARY

The *DSC* study indicates that the 58Bi-42Sn melts at about 140° C and solidifies at about 125° C, under a heating and cooling rate of 40° C/min. The eutectic 63Sn-37Pb and 52In-48Sn solders also have undercooling (defined as the difference between the melting start temperature and solidification start temperature) of about 10–20° C. The non-eutectic 43Sn-43Pb-14Bi and 40In-40Sn-20Pb solders exhibit almost no undercooling.

58Bi-42Sn solder wets with Cu matrix at a comparable but lower degree than the 60Sn-40Pb, 52In-48Sn, 43Sn-43Pb-14Bi, and 40In-40Sn-20Pb solders. A 58Bi-42Sn solder joint has a typical lamella microstructure. The interfacial intermetallic compound with the Cu matrix seems to be the product of only Sn and Cu. Bi does not react with Cu.

58Bi-42Sn solder is the strongest in creep deformation among the five solders studied. Under the same shear stress level, the steady state shear strain rate is at least three orders of magnitude slower than that of the softest 52In-48Sn solder. 58Bi-42Sn solder has a better low-cycle fatigue resistance than the 52In48Sn solder, but not as good as the other three solders.

ACKNOWLEDGEMENT

The valuable discussions with Ms. P. A. Kramer and J. Freer, Lawrence Berkeley Laboratory, are greatly appreciated. This work was supported by Digital Equipment Co. under contract to the Lawrence Berkeley Laboratory.

APPENDIX I: Evaluation of Wetting Anglel α

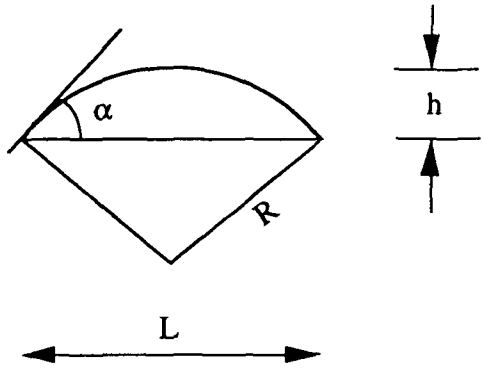

It is apparent from the above figure that,

$$\left(\frac{L}{2}\right)^2 + (R - h)^2 = R^2. \tag{1}$$

Solving R from Equation (1) leads to,

$$R = \frac{\left(\frac{L}{2}\right)^2 + h^2}{2h} \tag{2}$$

Also from the above figure, it is evident that,

$$\sin\alpha = \frac{L/2}{R} = \frac{2}{\frac{L/2}{h} + \frac{h}{L/2}} \tag{3}$$

By Eq. (3), the α value can be calculated from the measured values of L and h.

REFERENCES

1. L. Morrison, Electron. Prod. *16,* 33 (1987).
2. R. Strauss and S. Smernos, Circuit World *10,* 23 (1984).
3. S. Smernos and R. Strauss, Elect. Commun. *57,* 148 (1982).
4. R. Strauss and S. Smernos, The Bulletin of the Bismuth Institute *49,* 1 (1986).
5. R. J. K. Wassink, Soldering in Electronics, Electrochemical Publications Limited, 8 Barns Street, Ayr, Scotland, 1989, second Ed., p. 196.
6. Soldering Manual, American Welding Society, Inc., Miami, Florida 33125, 1978, second Ed., revised, pp. 10–11.
7. C. Lea, A Scientific Guide to Surface Mount Technology, Electrochemical Publications Limited, 8 Barns Street, Ayr, Scotland, 1988, p. 171.
8. Z. Mei and J. W. Morris, Jr., J. Electron. Mater., in press.
9. Binary Alloy Phase Diagrams, eds., Thaddeus B. Massalski et al., 1987, ASTM, Ohio, USA, vol. 1, and Max Hansen, Constitution of Binary Alloys, McGraw-Hill Book Company, New York/Toronto/London, 1958.
10. Soldering Manual, American Welding Society, Inc., Miami, Florida 33125, 1978, second Ed., revised, pp. 134–135.
11. J. S. Hwang, Solder Paste in Electronics Packaging, Van Nostrand Reinhold, New York, NY 10003, 1989, p. 115.
12. R. N. Wild, Nepcon Proceeding, 1974, pp. 105–117.
13. A. K. Covington, K. Groenwolt and B. W. Howlett, J. Inst. Met. *89,* 291 (1960).
14. B. F. Dyson, T. R. Anthony and D. Turnbull, J. Appl. Phys. *38,* 3408 (1967).
15. B. F. Dyson, T. R. Anthony and D. Turnbull, J. Appl. Phys. *37,* 2370 (1966).
16. B. F. Dyson, J. Appl. Phys. *37,* 2375 (1966).
17. Z. Mei, D. Grivas, M. C. Shine and J. W. Morris, Jr., J. Electron. Mater. *19,* 1273 (1990).
18. Z. Mei, J. W. Morris, Jr. and M. C. Shine, Trans. ASME-J. Electron. Packaging *113,* 109 (1991).
19. Metals Handbook, vol. 8, American Society for Metals, Metals Park, Ohio 44073, 1985, 9th Ed., p. 304.
20. J. E. Bird, A. K. Mukherjee and J. E. Dorn, Quantitative Relation Between Properties and Microstructure, eds., D. G. Brandon and A. Rosen, Israel University Press, Haifa, 1969.
21. Z. Mei, J. W. Morris, Jr., M. C. Shine and T. S. E. Summers, J. Electron. Mater. *20,* 599 (1991).
22. Z. Mei and J. W. Morris, Jr., ASME Winter Meeting, 1991, Atlanta, Georgia.
23. H. D. Solomon, Electronic Packaging Materials Science IV, eds., R. Jaccodine, K. A. Jackson, E. D. Lillie and R. C. Sundahl, MRS, Pittsburgh, Pennsylvania, 1989, pp. 441–451.
24. S. S. Manson, Mech. Des. *32,* 139 (1960).
25. L. F. Coffin, Jr. and J. F. Tavernelli, Trans. AIME *215,* 794 (1959).
26. H. D. Solomon, Trans. IEEE CHMT, Dec. 1986.
27. C. E. Pearson, J. Inst. Metals *54,* 111 (1934).